光学学报

部分相干圆刃型位错光束在生物组织中的偏振特性

贺改梅，段美玲*，殷子昂，单晶，冯姣姣
中北大学半导体与物理学院，山西 太原 030051

摘要 以推导的在生物组织中部分相干圆刃型位错光束传输时的交叉谱密度矩阵元，研究了传输中不同光束参数（光束波长λ、位错数目n_{dis}、空间自相关长度σ_{yy}）对不同场点之间偏振特性的影响。部分相干圆刃型位错光束波长和位错数目不影响偏振态的初始值，而不同空间自相关长度的光束初始偏振态不同。随着传输距离增加，空间同一点的偏振态经历明显的起伏变化后最终趋于与源处一致，空间不同两点间的偏振态最终趋于一不同于初始值的定值。与远红外光和紫外光相比，可见光和近红外光更适合作为生物医学疾病诊疗的目标光束。位错数目越大，各偏振特征参量极值间距越大。空间自相关长度σ_{yy}与σ_{xx}的相对大小会影响偏振度的大小及变化趋势。

关键词 生物光学；圆刃型位错光束；偏振度；方位角；椭圆率；生物组织
中图分类号 O436.3 **文献标志码** A **DOI**：10.3788/AOS231158

1 引 言

近年来，随着激光光学技术的迅速发展，光学方法在光声成像、光声学和生物医学光子学等领域的应用备受关注[1-3]，激光在生物组织中的传输行为也被广泛研究[4-5]。对生物组织中激光传输规律的模拟与检验可获取组织光学特性参数与漫反射率、漫透射率和通量等物理量间的关系，为组织诊断光谱学、辐射剂量学等的发展提供有效而严密的数学手段[6]。目前，大量学者研究了激光束在不同介质传输中的偏振行为，例如：乔文龙等[7]观察了生物组织中不同类型偏振光传输时后向散射光偏振变化与波长之间的联系，指出当波长相同时圆偏振光比线性偏振光能更好地保持其偏振性，故圆偏振光较多用于生物组织生理信息的检测；Zhou等[8]研究了有畸变的部分相干双曲余弦-艾里光束在海洋湍流中的传输特性，通过数值模拟对光束的平均光强、光谱相干性和偏振性进行了系统分析；Li等[9]分析了各向同性和各向异性光束在水平各向异性湍流传输中的偏振变化，研究发现光束的偏振特性和光源相干性有较强关联，由各向异性光源产生的光束通过一定长度的传输距离后，其偏振度恢复到初始值，而由各向同性光源产生的光束在较长的传输距离内可保持偏振度不变；Li等[10]研究了部分偏振、部分相干脉冲电磁光束通过各向异性湍流时偏振态的变化，详细讨论了各向异性湍流参数对光束偏振度、方位角和椭圆率的影响；陈康等[11]探究了径向阶数、拓扑荷数和相干宽度等参数对部分相干径向偏振旋转对称幂指数相位涡旋光束相干度和偏振度分布特点的影响。

奇点光学是光学的一个新分支，它研究波场中与相位奇异性（波前位错）有关的一系列效应。奇点光束相比于普通高斯光束在光信息载体中增加了一个全新的电磁维度——轨道角动量自由度，具有光强为零、相位不确定和螺旋状波前结构等特殊性质，传输中可以大幅提高信息传输容量。圆刃型位错在横平面内沿着传输方向有圆形切口，通过该切口的相位产生π突变，是典型的具有相位奇异性的奇点光束性质。Vasnetsov课题组[12-13]的研究显示，两束单轴高斯光束干涉可形成波前圆刃型位错，对此结构光束传输特性的研究屡见不鲜。Gao等[14]对比分析了圆刃型位错光束和圆-线刃型位错光束在不同介质中的传输，结果表明，在自由空间或大气湍流传输中，圆-线刃型位错光束中的圆刃型位错消失或演化为一对光学涡旋，而圆刃型位错光束在自由空间传输中稳定存在，在大气湍流传输中则演化为一对光学涡旋。Liu等[15]研究了非局域介质中圆-线刃型位错光束的非线性传输特性，详细讨论了光束宽度、曲率和强度分布的演化过程。Li等[16]通过数值模拟发现，大气湍流中圆刃型位错半径和数量以及湍流结构常数影响了光涡旋的演化。然

收稿日期：2023-06-20；**修回日期**：2023-08-05；**录用日期**：2023-09-15；**网络首发日期**：2023-09-22
基金项目：国家自然科学基金（12204439）
通信作者：*meilingduan@nuc.edu.cn

而，目前关于圆刃型位错光束在生物组织传输中偏振态的研究甚少，此研究将推动奇点光束在组织成像、生物医学疾病诊断等应用的发展。

本文推导了部分相干圆刃型位错光束在生物组织传输中的交叉谱密度矩阵，对光束偏振度、方位角和椭圆率的变化进行了数值计算，分析了光束波长 λ、位错数目 n_{dis} 和空间自相关长度 σ_{yy} 对两种场点间偏振度、方位角、椭圆率变化的影响。

2 理论模型

根据光的相干与偏振统一理论，圆刃型位错光束在 $z=0$（源平面）处的交叉谱密度矩阵[17-18]为

$$\boldsymbol{W}(\boldsymbol{s}_1,\boldsymbol{s}_2,0)=\begin{pmatrix} W_{xx}(\boldsymbol{s}_1,\boldsymbol{s}_2,0) & W_{xy}(\boldsymbol{s}_1,\boldsymbol{s}_2,0)\\ W_{yx}(\boldsymbol{s}_1,\boldsymbol{s}_2,0) & W_{yy}(\boldsymbol{s}_1,\boldsymbol{s}_2,0)\end{pmatrix},\tag{1}$$

$$W_{ij}(\boldsymbol{s}_1,\boldsymbol{s}_2,0)=\left\langle E_i^*(\boldsymbol{s}_1,0)\cdot E_j(\boldsymbol{s}_2,0)\right\rangle (i,j=x,y),\tag{2}$$

式中：E_x 和 E_y 表示直角坐标系中 x、y 方向的电场分量；$\boldsymbol{s}_l=(s_{lx},s_{ly})(l=1,2)$ 为源平面处的两点位置矢量；* 表示复共轭；$\langle\cdot\rangle$ 为系综平均。

假设 $\mathrm{H}_n(\cdot)$ 表示阶数为 n 的厄米特多项式，则圆刃型位错光束在 $z=0$ 处的场分布[19]为

$$E(\boldsymbol{s},0)=\frac{(-1)^n}{2^{2n}(n!)}\sum_{t=0}^{n}\binom{n}{t}\mathrm{H}_{2t}\left(\frac{\sqrt{2}\,s_x}{w_0}\right)\mathrm{H}_{2n-2t}\left(\frac{\sqrt{2}\,s_y}{w_0}\right)\exp\left(-\frac{\boldsymbol{s}^2}{{w_0}^2}\right),\tag{3}$$

引入谢尔项[20]，可得到部分相干圆刃型位错光束在 $z=0$ 处的交叉谱密度矩阵元为

$$W_{ij}(\boldsymbol{s}_1,\boldsymbol{s}_2,0)=\left\langle E_i^*E_j\right\rangle=A_iA_jB_{ij}\frac{1}{2^{4n}(n!)^2}\sum_{t_1=0}^{n}\sum_{t_2=0}^{n}\binom{n}{t_1}\binom{n}{t_2}\exp\left(-\frac{{\boldsymbol{s}_1}^2+{\boldsymbol{s}_2}^2}{{w_0}^2}\right)\times$$
$$\mathrm{H}_{2t_1}\left(\frac{\sqrt{2}\,s_{1x}}{w_0}\right)\mathrm{H}_{2n-2t_1}\left(\frac{\sqrt{2}\,s_{1y}}{w_0}\right)\mathrm{H}_{2t_2}\left(\frac{\sqrt{2}\,s_{2x}}{w_0}\right)\mathrm{H}_{2n-2t_2}\left(\frac{\sqrt{2}\,s_{2y}}{w_0}\right)\exp\left(-\frac{(\boldsymbol{s}_1-\boldsymbol{s}_2)^2}{2{\sigma_{ij}}^2}\right),\tag{4}$$

式中：A_i 和 A_j 分别表示电场分量 E_i 和 E_j 的振幅；B_{ij} 为光源平面 E_i 和 E_j 之间的相位相关因子；w_0 为束腰宽度；σ_{xx} 和 σ_{yy} 为空间自相关长度；σ_{xy} 和 σ_{yx} 为空间互相关长度。

根据广义惠更斯-菲涅耳原理[21]，部分相干圆刃型位错光束在生物组织传输中的交叉谱密度矩阵元为

$$W_{ij}(\boldsymbol{\rho}_1,\boldsymbol{\rho}_2,z)=\left(\frac{k}{2\pi z}\right)^2\iiiint W_{ij}(\boldsymbol{s}_1,\boldsymbol{s}_2,0)\exp\left\{-\frac{\mathrm{i}k}{2z}\left[(\boldsymbol{s}_1-\boldsymbol{\rho}_1)^2-(\boldsymbol{s}_2-\boldsymbol{\rho}_2)^2\right]\right\}\times$$
$$\left\langle\exp\left[\psi^*(\boldsymbol{\rho}_1,\boldsymbol{s}_1)+\psi(\boldsymbol{\rho}_2,\boldsymbol{s}_2)\right]\right\rangle\mathrm{d}\boldsymbol{s}_1\mathrm{d}\boldsymbol{s}_2,\tag{5}$$

式中：$\boldsymbol{\rho}_1=(\rho_{1x},\rho_{1y})$、$\boldsymbol{\rho}_2=(\rho_{2x},\rho_{2y})$ 是传输平面上的两点；k 为波数，与波长 λ 的关系为 $k=2\pi/\lambda$；$\left\langle\exp\left[\psi^*(\boldsymbol{\rho}_1,\boldsymbol{s}_1)+\psi(\boldsymbol{\rho}_2,\boldsymbol{s}_2)\right]\right\rangle$ 表示湍流介质扰动引起的相位起伏[22]，表示为

$$\left\langle\exp\left[\psi^*(\boldsymbol{\rho}_1,\boldsymbol{s}_1)+\psi(\boldsymbol{\rho}_2,\boldsymbol{s}_2)\right]\right\rangle=\exp\left\{-4\pi^2k^2z\int_0^1\mathrm{d}t\int_0^\infty\mathrm{d}\kappa\kappa\Phi(\kappa)\left\{1-\mathrm{J}_0\left[\left|t(\boldsymbol{\rho}_1-\boldsymbol{\rho}_2)+(1-t)(\boldsymbol{s}_1-\boldsymbol{s}_2)\right|\kappa\right]\right\}\right\},\tag{6}$$

式中：$\Phi(\kappa)$ 为扰动介质的折射率功率谱。对哺乳动物而言，折射率功率谱的表达式[23]为

$$\Phi(\kappa)=\frac{4\pi\left\langle\delta n_{\mathrm{RI}}^2\right\rangle L_0^2(\zeta-1)}{(1+\kappa^2L_0^2)^\zeta},\tag{7}$$

式中：L_0 为折射率的外尺寸；ζ 与生物组织的分形维数有关，表征生物组织的扰动大小；$\left\langle\delta n_{\mathrm{RI}}^2\right\rangle$ 为折射率的均方。

式(6)中，$\mathrm{J}_0(x)$ 为零阶贝塞尔函数，取前两项作为其近似表达[24]，式(6)可表示为

$$\left\langle\exp\left[\psi^*(\boldsymbol{\rho}_1,\boldsymbol{s}_1)+\psi(\boldsymbol{\rho}_2,\boldsymbol{s}_2)\right]\right\rangle\approx\exp\left\{-\frac{1}{{\rho_0}^2}\left[(\boldsymbol{s}_1-\boldsymbol{s}_2)^2+(\boldsymbol{\rho}_1-\boldsymbol{\rho}_2)^2+(\boldsymbol{s}_1-\boldsymbol{s}_2)(\boldsymbol{\rho}_1-\boldsymbol{\rho}_2)\right]\right\},\tag{8}$$

式中：ρ_0 描述球面波在介质传输中的相关长度。对于生物组织，相关长度的表达式为

$$\left|\rho_0(z)\right|=0.22(C_{n_{\mathrm{RI}}}^2k^2z)^{-1/2},\tag{9}$$

式中：$C_{n_{\mathrm{RI}}}^2$ 为生物组织的折射率结构常数，其表达式为

$$C_{n_{\mathrm{RI}}}^2=\frac{\left\langle\delta n_{\mathrm{RI}}^2\right\rangle}{L_0^2(2-\zeta)}。\tag{10}$$

由文献[23]可得几种生物组织样本的折射率结构常数。

利用厄米函数的性质及积分公式[25]

$$\int \exp\left[-(x-y)^2\right] \mathrm{H}_n(ax)\,\mathrm{d}x = \sqrt{\pi}\,(1-a^2)^{\frac{n}{2}} \mathrm{H}_n\left[\frac{ay}{(1-a^2)^{\frac{1}{2}}}\right], \tag{11}$$

$$\int x^n \exp\left[-(x-\beta)^2\right] \mathrm{d}x = (2\mathrm{i})^{-n}\sqrt{\pi}\,\mathrm{H}_n(\mathrm{i}\beta), \tag{12}$$

$$\mathrm{H}_n(x) = \sum_{m=0}^{[n/2]} (-1)^m \frac{n!}{m!(n-2m)!}(2x)^{n-2m}, \tag{13}$$

$$\mathrm{H}_n(x+y) = \frac{1}{2^{n/2}} \sum_{k=0}^{n} \binom{n}{k} \mathrm{H}_k\left(\sqrt{2}\,x\right) \mathrm{H}_{n-k}\left(\sqrt{2}\,y\right), \tag{14}$$

式(5)可写成

$$W_{ij}(\boldsymbol{\rho}_1, \boldsymbol{\rho}_2, z) = A_i A_j B_{ij} \exp\left[-\frac{\mathrm{i}k}{2z}\left(\boldsymbol{\rho}_1^{\,2} - \boldsymbol{\rho}_2^{\,2}\right) - \frac{1}{\boldsymbol{\rho}_0^{\,2}}\left(\boldsymbol{\rho}_1 - \boldsymbol{\rho}_2\right)^2\right] \times \left(\frac{k}{2\pi z}\right)^2 \frac{1}{2^{4n}(n!)^2} P_{ij} E_{ij} \sum_{t_1=0}^{n}\sum_{t_2=0}^{n} \binom{n}{t_1}\binom{n}{t_2} N_{ij} M_{ij}, \tag{15}$$

$$P_{ij} = \exp\left\{\frac{1}{4D_{ij}}\left[\frac{\boldsymbol{\rho}_1^2 + \boldsymbol{\rho}_2^2}{\rho_0^4} - \frac{\left(2z + 2\mathrm{i}k\rho_0^2\right)\left(\rho_{1x}\rho_{2x} + \rho_{1y}\rho_{2y}\right)}{\rho_0^4 z} + \frac{\left(2\mathrm{i}kz - k^2\rho_0^2\right)\boldsymbol{\rho}_2^2}{\rho_0^2 z^2}\right]\right\}, \tag{16}$$

$$N_{ij} = \sum_{c_1=0}^{[t_1]} \sum_{d_1=0}^{2t_2} \sum_{e_1=0}^{\left[\frac{d_1}{2}\right]} \binom{2t_2}{d_1} (-1)^{c_1+e_1} (2\mathrm{i})^{-(2t_1-2c_1+d_1-2e_1)} \frac{(2t_1)!}{c_1!(2t_1-2c_1)!} \frac{d_1!}{e_1!(d_1-2e_1)!} \times$$
$$\frac{\pi}{\sqrt{D_{ij}}}\left(1-\frac{2}{w_0^2 D_{ij}}\right)^{t_2} 2^{-t_2}\left[\frac{2\left(\rho_0^2+2\sigma_0^2\right)}{\rho_0^2\sigma_{ij}^2\sqrt{w_0^2 D_{ij}^{\,2} - 2D_{ij}}}\right]^{d_1-2e_1} \left(\frac{1}{\sqrt{G_{ij}}}\right)^{2t_1-2c_1+d_1-2e_1+1} \times$$
$$\left(\frac{2\sqrt{2}}{w_0}\right)^{2t_1-2c_1} \mathrm{H}_{2t_2-d_1}\left[\frac{\left(\rho_{1x}-\rho_{2x}\right)z - \mathrm{i}k\rho_{2x}\rho_0^2}{\rho_0^2 z\sqrt{w_0^2 D_{ij}^{\,2} - 2D_{ij}}}\right] \mathrm{H}_{2t_1-2c_1+d_1-2e_1}\left(\mathrm{i}\frac{F_{ijx}}{2\sqrt{G_{ij}}}\right), \tag{17}$$

$$M_{ij} = \sum_{c_2=0}^{[n-t_1]} \sum_{d_2=0}^{2n-2t_2} \sum_{e_2=0}^{\left[\frac{d_2}{2}\right]} \binom{2n-2t_2}{d_2} (-1)^{c_2+e_2} \frac{(2n-2t_1)!}{c_2!(2n-2t_1-2c_2)!} \frac{d_2!}{e_2!(d_2-2e_2)!} \times$$
$$(2\mathrm{i})^{-(2n-2t_1-2c_2+d_2-2e_2)} 2^{-(n-t_2)}\left(1-\frac{2}{w_0^2 D_{ij}}\right)^{n-t_2}\left[\frac{2\left(\rho_0^2+2\sigma_0^2\right)}{\rho_0^2\sigma_{ij}^2\sqrt{w_0^2 D_{ij}^{\,2} - 2D_{ij}}}\right]^{d_2-2e_2} \frac{\pi}{\sqrt{D_{ij}}}\left(\frac{2\sqrt{2}}{w_0}\right)^{2n-2t_1-2c_2} \times$$
$$\left(\frac{1}{\sqrt{G_{ij}}}\right)^{2n-2t_1-2c_2+d_2-2e_2+1} \times \mathrm{H}_{2n-2t_2-d_2}\left[\frac{\left(\rho_{1y}-\rho_{2y}\right)z - \mathrm{i}k\rho_{2y}\rho_0^2}{\rho_0^2 z\sqrt{w_0^2 D_{ij}^{\,2} - 2D_{ij}}}\right] \mathrm{H}_{2n-2t_1-2c_2+d_2-2e_2}\left(\mathrm{i}\frac{F_{ijy}}{2\sqrt{G_{ij}}}\right), \tag{18}$$

$$E_{ij} = \exp\left[\frac{1}{4G_{ij}}\left(F_{ijx}^2 + F_{ijy}^2\right)\right], \tag{19}$$

$$D_{ij} = \frac{1}{w_0^2} + \frac{1}{2\sigma_{ij}^2} - \frac{\mathrm{i}k}{2z} + \frac{1}{\rho_0^2}, \tag{20}$$

$$F_{ijx} = \frac{\mathrm{i}k\rho_{1x}}{z} - \frac{\rho_{1x}-\rho_{2x}}{\rho_0^2} + \frac{1}{2D_{ij}}\left(\frac{1}{\sigma_{ij}^2} + \frac{2}{\rho_0^2}\right)\left(\frac{\rho_{1x}-\rho_{2x}}{\rho_0^2} - \frac{\mathrm{i}k\rho_{2x}}{z}\right), \tag{21}$$

$$G_{ij} = \frac{1}{w_0^2} + \frac{1}{2\sigma_{ij}^2} + \frac{\mathrm{i}k}{2z} + \frac{1}{\rho_0^2} - \frac{1}{4D_{ij}}\left(\frac{1}{\sigma_{ij}^2} + \frac{2}{\rho_0^2}\right)^2。 \tag{22}$$

根据对称性,将F_{ijx}中的ρ_x换成ρ_y即得F_{ijy}。描述光束偏振态的3个参量可表示为

$$P(\boldsymbol{\rho}_1, \boldsymbol{\rho}_2, z) = \sqrt{1 - 4\mathrm{Det}\boldsymbol{W}(\boldsymbol{\rho}_1, \boldsymbol{\rho}_2, z) \Big/ \left[\mathrm{Tr}\boldsymbol{W}(\boldsymbol{\rho}_1, \boldsymbol{\rho}_2, z)\right]^2}, \tag{23}$$

$$\theta(\boldsymbol{\rho}_1, \boldsymbol{\rho}_2, z) = \frac{1}{2}\arctan\left\{\frac{2\mathrm{Re}\left[W_{xy}(\boldsymbol{\rho}_1, \boldsymbol{\rho}_2, z)\right]}{W_{xx}(\boldsymbol{\rho}_1, \boldsymbol{\rho}_2, z) - W_{yy}(\boldsymbol{\rho}_1, \boldsymbol{\rho}_2, z)}\right\}, \tag{24}$$

$$\varepsilon(\boldsymbol{\rho}_1, \boldsymbol{\rho}_2, z) = A_{\mathrm{minor}} / A_{\mathrm{major}} \quad (0 \leqslant \varepsilon \leqslant 1), \tag{25}$$

式中：$P(\boldsymbol{\rho}_1,\boldsymbol{\rho}_2,z)$为交叉偏振度[26]；$\theta(\boldsymbol{\rho}_1,\boldsymbol{\rho}_2,z)$为方位角[27]；$\varepsilon(\boldsymbol{\rho}_1,\boldsymbol{\rho}_2,z)$为椭圆率[28]；Det$|\boldsymbol{W}|$和Tr$|\boldsymbol{W}|$分别为矩阵$\boldsymbol{W}$的秩和迹；$A_{\mathrm{minor}}$和$A_{\mathrm{major}}$分别表示偏振椭圆的长半轴和短半轴。

$$A^2_{\mathrm{minor}}(\boldsymbol{\rho}_1,\boldsymbol{\rho}_2,z)=\left[\sqrt{(W_{xx}-W_{yy})^2+4\left|W_{xy}\right|^2}-\sqrt{(W_{xx}-W_{yy})^2+4\left|\mathrm{Re}\,W_{xy}\right|^2}\right]\Big/2, \tag{26}$$

$$A^2_{\mathrm{major}}(\boldsymbol{\rho}_1,\boldsymbol{\rho}_2,z)=\left[\sqrt{(W_{xx}-W_{yy})^2+4\left|W_{xy}\right|^2}+\sqrt{(W_{xx}-W_{yy})^2+4\left|\mathrm{Re}\,W_{xy}\right|^2}\right]\Big/2。 \tag{27}$$

由式(23)～(25)可分析光束在生物组织传输中的偏振态变化。

3　数值分析

光束偏振态是描述光场的重要统计量之一，传输中光束偏振态的变化是很重要的信息，如在受激辐射损耗荧光显微技术中，与入射受激场的偏振态相关的线性分子偶极跃迁的方向对空间分辨率有很大影响[29]。下面研究部分相干圆刃型位错光束在人体真皮组织传输中不同光束参数(波长λ、位错数目n_{dis}和空间自相关长度σ_{yy})和传输距离z对同一场点及两个不同场点间的偏振态变化的影响。本文选取计算样本的折射率结构常数为$C^2_{n_{\mathrm{kl}}}=0.44\times10^{-3}\ \mu\mathrm{m}^{-1}$[23]。

3.1　波长的影响

图1所示为人体真皮组织中不同λ的部分相干圆刃型位错光束传输时偏振度$P(\boldsymbol{\rho},0,z)$和$P(\boldsymbol{\rho},\boldsymbol{\rho},z)$随$z$的变化。计算参数为$A_x=A_y=(0.5)^{1/2}$、$B_{xy}=B^*_{yx}=0.3\exp(\mathrm{i}\pi/3)$、$B_{xx}=B_{yy}=1$、$\boldsymbol{\rho}=(0.2\ \mu\mathrm{m},0)$、$n_{\mathrm{dis}}=1$、$w_0=2\ \mu\mathrm{m}$、$\sigma_{xx}=0.15\ \mu\mathrm{m}$、$\sigma_{xy}=\sigma_{yx}=0.25\ \mu\mathrm{m}$、$\sigma_{yy}=0.225\ \mu\mathrm{m}$。选取4种不同波长的光束进行讨论，分别为紫外光($\lambda=0.325\ \mu\mathrm{m}$)、可见光($\lambda=0.6328\ \mu\mathrm{m}$)、近红外光($\lambda=0.83\ \mu\mathrm{m}$)、远红外光($\lambda=10\ \mu\mathrm{m}$)。由图1可知，$P(\boldsymbol{\rho},0,z)$的初始值大于$P(\boldsymbol{\rho},\boldsymbol{\rho},z)$的初始值，经过一定的传输距离，$P(\boldsymbol{\rho},0,z)$最终趋于定值，且小于其初始值，而$P(\boldsymbol{\rho},\boldsymbol{\rho},z)$最终趋于其初始值。传输中$P(\boldsymbol{\rho},0,z)$和$P(\boldsymbol{\rho},\boldsymbol{\rho},z)$都发生了显著的起伏变化，$P(\boldsymbol{\rho},0,z)$出现两次极大值和两次极小值，$P(\boldsymbol{\rho},\boldsymbol{\rho},z)$出现两次极大值和一次极小值。$\lambda$越大，每次达到的极值越大，$P(\boldsymbol{\rho},0,z)$和$P(\boldsymbol{\rho},\boldsymbol{\rho},z)$趋于定值的传输距离越远。此外，远红外光束在一段传输距离内，$P(\boldsymbol{\rho},0,z)$和$P(\boldsymbol{\rho},\boldsymbol{\rho},z)$几乎保持一极值，这可能是因为远红外光束的波长与生物组织发射的波长非常接近，在传输过程中与生物组织中的水分子发生了共振。在初始值相同的条件下，传输中紫外光的偏振度最小，可能原因为紫外光被生物组织强烈吸收；可见光和近红外光的偏振度变化介于紫外光与远红外光之间。

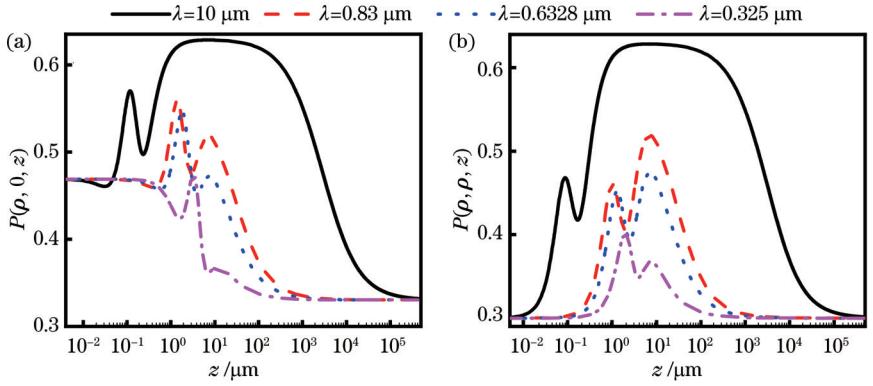

图1　具有不同波长的光束偏振度P随z的变化。(a)$P(\boldsymbol{\rho},0,z)$；(b)$P(\boldsymbol{\rho},\boldsymbol{\rho},z)$

Fig. 1　Change of the degree of polarization P with z for beams with different wavelengths. (a) $P(\boldsymbol{\rho},0,z)$; (b) $P(\boldsymbol{\rho},\boldsymbol{\rho},z)$

图2所示为方位角$\theta(\boldsymbol{\rho},0,z)$和$\theta(\boldsymbol{\rho},\boldsymbol{\rho},z)$随$z$的变化，计算参数同图1。由图2可知：$\theta(\boldsymbol{\rho},0,z)$的初始值大于$\theta(\boldsymbol{\rho},\boldsymbol{\rho},z)$的初始值；随着传输距离增加，$\theta(\boldsymbol{\rho},0,z)$和$\theta(\boldsymbol{\rho},\boldsymbol{\rho},z)$的变化趋势不同。起始传输中，$\theta(\boldsymbol{\rho},0,z)$先减小后增大，$\theta(\boldsymbol{\rho},\boldsymbol{\rho},z)$先增大后减小；$\lambda$越大，各自极值出现越早，极值越大。最终$\theta(\boldsymbol{\rho},0,z)$和$\theta(\boldsymbol{\rho},\boldsymbol{\rho},z)$分别趋于一定值，且$\theta(\boldsymbol{\rho},0,z)$的趋向值小于初始值，$\theta(\boldsymbol{\rho},\boldsymbol{\rho},z)$趋向值与初始值一致。此外，$\theta(\boldsymbol{\rho},0,z)$和$\theta(\boldsymbol{\rho},\boldsymbol{\rho},z)$的变化也有类似于$P(\boldsymbol{\rho},0,z)$和$P(\boldsymbol{\rho},\boldsymbol{\rho},z)$的在一段传输距离内维持某一极值的现象。

图3所示为椭圆率$\varepsilon(\boldsymbol{\rho},0,z)$和$\varepsilon(\boldsymbol{\rho},\boldsymbol{\rho},z)$随$z$的变化，计算参数同图1。由图3可知，传输中，$\varepsilon(\boldsymbol{\rho},0,z)$和$\varepsilon(\boldsymbol{\rho},\boldsymbol{\rho},z)$的变化趋势相似。$\varepsilon(\boldsymbol{\rho},0,z)$的初始值小于$\varepsilon(\boldsymbol{\rho},\boldsymbol{\rho},z)$的初始值，经过一段传输距离后，$\varepsilon(\boldsymbol{\rho},0,z)$和$\varepsilon(\boldsymbol{\rho},\boldsymbol{\rho},z)$在生物组织中分别趋于不同的定值，且$\varepsilon(\boldsymbol{\rho},0,z)$的趋向值大于初始值，$\varepsilon(\boldsymbol{\rho},\boldsymbol{\rho},z)$最终趋于初始值，且$\varepsilon(\boldsymbol{\rho},0,z)$的趋向值小于$\varepsilon(\boldsymbol{\rho},\boldsymbol{\rho},z)$

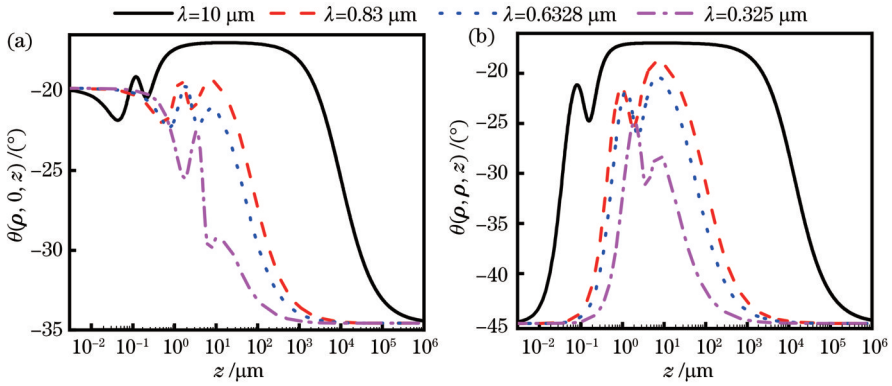

图 2　具有不同波长的光束方位角 θ 随 z 的变化。(a)$\theta(\boldsymbol{\rho}, 0, z)$;(b)$\theta(\boldsymbol{\rho}, \boldsymbol{\rho}, z)$

Fig. 2　Change of orientation angle θ with z for beams with different wavelengths. (a) $\theta(\boldsymbol{\rho}, 0, z)$; (b) $\theta(\boldsymbol{\rho}, \boldsymbol{\rho}, z)$

的趋向值。λ 越大,$\varepsilon(\boldsymbol{\rho}, 0, z)$ 和 $\varepsilon(\boldsymbol{\rho}, \boldsymbol{\rho}, z)$ 的极值越小。此外,$\varepsilon(\boldsymbol{\rho}, 0, z)$ 和 $\varepsilon(\boldsymbol{\rho}, \boldsymbol{\rho}, z)$ 的变化也有类似于 $\theta(\boldsymbol{\rho}, 0, z)$ 和 $\theta(\boldsymbol{\rho}, \boldsymbol{\rho}, z)$、$P(\boldsymbol{\rho}, 0, z)$ 和 $P(\boldsymbol{\rho}, \boldsymbol{\rho}, z)$ 的在一段传输距离内维持某一极值的现象。由图 1~3 可知,在生物组织传输中,可见光和近红外光的偏振态变化幅度适中,变化规律相近,故通常被作为光学方法应用于生物医学疾病诊疗的候选光波。

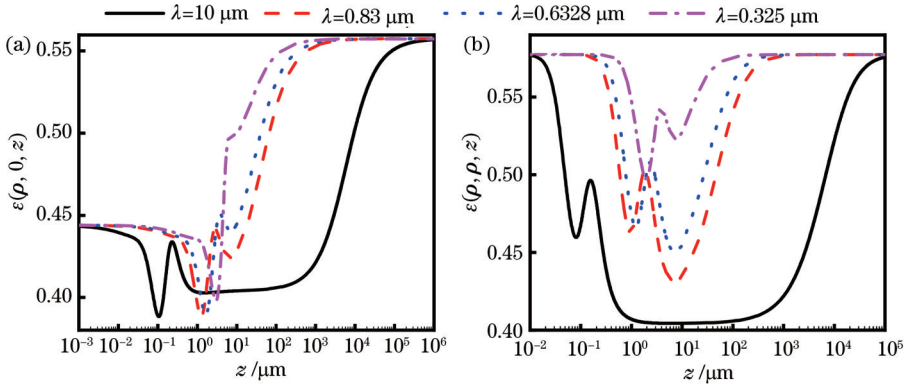

图 3　具有不同波长的光束椭圆率 ε 随 z 的变化。(a)$\varepsilon(\boldsymbol{\rho}, 0, z)$;(b)$\varepsilon(\boldsymbol{\rho}, \boldsymbol{\rho}, z)$

Fig. 3　Change of ellipticity ε with z for beams with different wavelengths. (a) $\varepsilon(\boldsymbol{\rho}, 0, z)$; (b) $\varepsilon(\boldsymbol{\rho}, \boldsymbol{\rho}, z)$

3.2　位错数目的影响

图 4 所示为人体真皮组织中不同 n 的部分相干圆刃型位错光束传输时 $P(\boldsymbol{\rho}, 0, z)$ 和 $P(\boldsymbol{\rho}, \boldsymbol{\rho}, z)$ 随 z 的变化,计算参数 $\lambda=0.6328$ μm,其他参数同图 1。由图 4 可知:n 对起始偏振度的影响可忽略,$P(\boldsymbol{\rho}, 0, z)$ 的初始值大于 $P(\boldsymbol{\rho}, \boldsymbol{\rho}, z)$ 的初始值;传输中,$P(\boldsymbol{\rho}, 0, z)$ 达到两次极小值和两次极大值,$P(\boldsymbol{\rho}, \boldsymbol{\rho}, z)$ 达到一次极小值和两次极大值。n_{dis} 越小,同次的极值越大,$P(\boldsymbol{\rho}, 0, z)$ 越早到达极值,$P(\boldsymbol{\rho}, \boldsymbol{\rho}, z)$ 越晚到达极值。当 $z>10^3$ μm 时,$P(\boldsymbol{\rho}, 0, z)$ 和 $P(\boldsymbol{\rho}, \boldsymbol{\rho}, z)$ 分别趋于不同的定值,且 $P(\boldsymbol{\rho}, 0, z)$ 最终趋于一小于初始值的定值,$P(\boldsymbol{\rho}, \boldsymbol{\rho}, z)$ 最终趋于初始值。

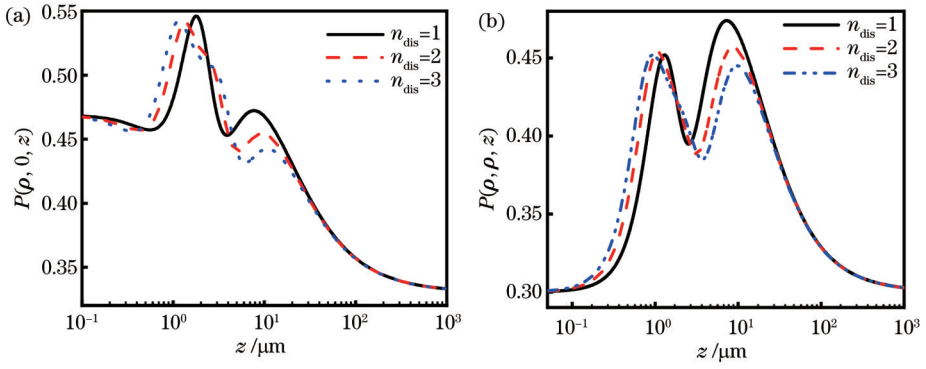

图 4　具有不同位错数目的光束偏振度 P 随 z 的变化。(a)$P(\boldsymbol{\rho}, 0, z)$;(b)$P(\boldsymbol{\rho}, \boldsymbol{\rho}, z)$

Fig. 4　Change of the degree of polarization P with z for beams with different numbers of dislocations. (a) $P(\boldsymbol{\rho}, 0, z)$; (b) $P(\boldsymbol{\rho}, \boldsymbol{\rho}, z)$

图 5 所示为 $\theta(\boldsymbol{\rho}, 0, z)$ 和 $\theta(\boldsymbol{\rho}, \boldsymbol{\rho}, z)$ 随 z 的变化，计算参数同图 4。由图 5 可知：$\theta(\boldsymbol{\rho}, 0, z)$ 的初始值大于 $\theta(\boldsymbol{\rho}, \boldsymbol{\rho}, z)$ 的初始值；n_{dis} 值增大，传输中 $\theta(\boldsymbol{\rho}, 0, z)$ 和 $\theta(\boldsymbol{\rho}, \boldsymbol{\rho}, z)$ 的极值减小，$\theta(\boldsymbol{\rho}, 0, z)$ 两个极小值的位置将远离，$\theta(\boldsymbol{\rho}, \boldsymbol{\rho}, z)$ 两个极大值的位置也将远离。$\theta(\boldsymbol{\rho}, 0, z)$ 最终趋于一小于初始值的定值，$\theta(\boldsymbol{\rho}, \boldsymbol{\rho}, z)$ 最终趋于初始值。

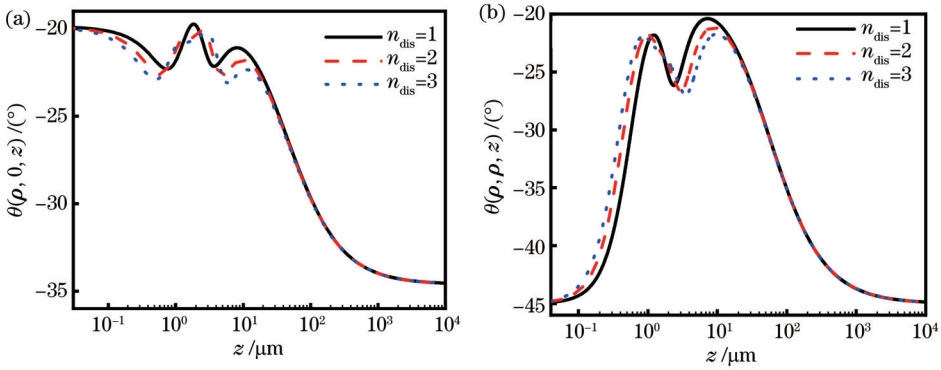

图 5　具有不同位错数目的光束方位角 θ 随 z 的变化。(a) $\theta(\boldsymbol{\rho}, 0, z)$；(b) $\theta(\boldsymbol{\rho}, \boldsymbol{\rho}, z)$

Fig. 5　Change of orientation angle θ with z for beams with different numbers of dislocations. (a) $\theta(\boldsymbol{\rho}, 0, z)$; (b) $\theta(\boldsymbol{\rho}, \boldsymbol{\rho}, z)$

图 6 所示为 $\varepsilon(\boldsymbol{\rho}, 0, z)$ 和 $\varepsilon(\boldsymbol{\rho}, \boldsymbol{\rho}, z)$ 随 z 的变化，计算参数同图 4。由图 6 可知：$\varepsilon(\boldsymbol{\rho}, 0, z)$ 的初始值小于 $\varepsilon(\boldsymbol{\rho}, \boldsymbol{\rho}, z)$ 的初始值；传输中 $\varepsilon(\boldsymbol{\rho}, 0, z)$ 和 $\varepsilon(\boldsymbol{\rho}, \boldsymbol{\rho}, z)$ 分别达到两次极小值和一次极大值；n_{dis} 越大，$\varepsilon(\boldsymbol{\rho}, 0, z)$ 和 $\varepsilon(\boldsymbol{\rho}, \boldsymbol{\rho}, z)$ 各自的两个极小值相距越远。经过一段传输距离，$\varepsilon(\boldsymbol{\rho}, 0, z)$ 趋于一大于初始值的定值，$\varepsilon(\boldsymbol{\rho}, \boldsymbol{\rho}, z)$ 最终趋于初始值，且 $\varepsilon(\boldsymbol{\rho}, 0, z)$ 到达定值晚于 $\varepsilon(\boldsymbol{\rho}, \boldsymbol{\rho}, z)$。由图 4～6 可知，根据激光束在生物组织传输中 $P(\boldsymbol{\rho}, 0, z)$、$P(\boldsymbol{\rho}, \boldsymbol{\rho}, z)$、$\theta(\boldsymbol{\rho}, 0, z)$、$\theta(\boldsymbol{\rho}, \boldsymbol{\rho}, z)$、$\varepsilon(\boldsymbol{\rho}, 0, z)$ 和 $\varepsilon(\boldsymbol{\rho}, \boldsymbol{\rho}, z)$ 的变化幅度、极值出现位置以及极值大小的差别，在不同应用中可选择不同位错数目的光束，从而降低产生激光束的复杂度，节约生产成本。

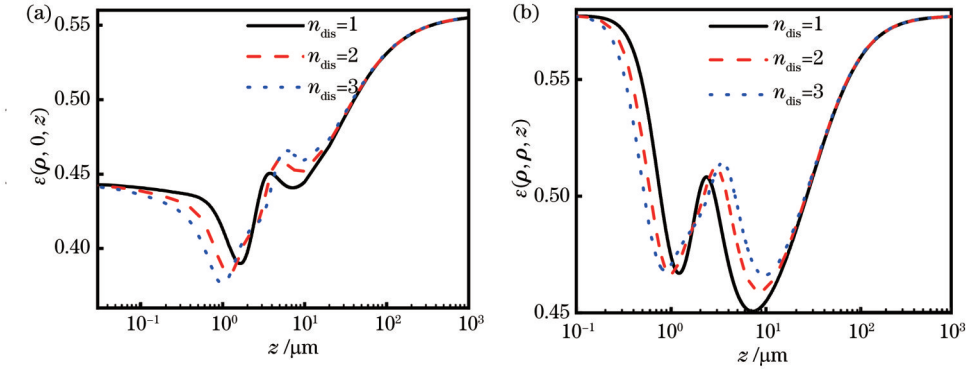

图 6　具有不同位错数目的光束椭圆率 ε 随 z 的变化。(a) $\varepsilon(\boldsymbol{\rho}, 0, z)$；(b) $\varepsilon(\boldsymbol{\rho}, \boldsymbol{\rho}, z)$

Fig. 6　Change of ellipticity ε with z for beams with different numbers of dislocations. (a) $\varepsilon(\boldsymbol{\rho}, 0, z)$; (b) $\varepsilon(\boldsymbol{\rho}, \boldsymbol{\rho}, z)$

3.3　空间自相关长度 σ_{yy} 的影响

图 7 所示为人体真皮组织中不同空间自相关长度 σ_{yy} 的部分相干圆刃型位错光束传输时 $P(\boldsymbol{\rho}, 0, z)$ 和 $P(\boldsymbol{\rho}, \boldsymbol{\rho}, z)$ 随 z 的变化，计算参数 λ=0.6328 μm，其他参数同图 1。由图 7 可知，对于不同 σ_{yy} 的光束，$P(\boldsymbol{\rho}, 0, z)$ 的初始值不同，但 $P(\boldsymbol{\rho}, \boldsymbol{\rho}, z)$ 的初始值不受影响。起始传输中，$P(\boldsymbol{\rho}, 0, z)$ 先减小再增大，$P(\boldsymbol{\rho}, \boldsymbol{\rho}, z)$ 逐渐增大。随着传输距离增大，不同 σ_{yy} 光束的 $P(\boldsymbol{\rho}, 0, z)$ 和 $P(\boldsymbol{\rho}, \boldsymbol{\rho}, z)$ 分别在相同位置达到各自极值，$P(\boldsymbol{\rho}, 0, z)$ 出现两次极大值和两次极小值，较近处的极大值大于较远处的极大值，而 $P(\boldsymbol{\rho}, \boldsymbol{\rho}, z)$ 出现两次极大值和一次极小值，较近处的极大值小于较远处的极大值。比较图 7(a)、(b)可知，σ_{yy} 相同的光束，$P(\boldsymbol{\rho}, 0, z)$ 的极大值大于 $P(\boldsymbol{\rho}, \boldsymbol{\rho}, z)$ 的极大值。当 $\sigma_{yy}<\sigma_{xx}$ 时，σ_{yy} 越小，$P(\boldsymbol{\rho}, 0, z)$ 和 $P(\boldsymbol{\rho}, \boldsymbol{\rho}, z)$ 在同一传输位置的数值越大；当 $\sigma_{yy}>\sigma_{xx}$ 且大于 0.225 μm 时，σ_{yy} 越大，二者在同一传输位置的数值越大，$P(\boldsymbol{\rho}, 0, z)$ 的趋向值小于初始值，$P(\boldsymbol{\rho}, \boldsymbol{\rho}, z)$ 的趋向值与初始值相等。

图 8 所示为 $\theta(\boldsymbol{\rho}, 0, z)$ 和 $\theta(\boldsymbol{\rho}, \boldsymbol{\rho}, z)$ 随 z 的变化，计算参数 λ=0.6328 μm，其他参数同图 1。当 $\sigma_{yy}=\sigma_{xx}$ 时，$W_{yy}=W_{xx}$，由式(24)可知，方位角没有意义。由图 8 可知，方位角的变化与 σ_{xx} 和 σ_{yy} 的相对大小有关。当 $\sigma_{yy}<\sigma_{xx}$ 时，$\theta(\boldsymbol{\rho}, 0, z)$ 和 $\theta(\boldsymbol{\rho}, \boldsymbol{\rho}, z)$ 为正，反之，二者均为负；σ_{yy} 与 σ_{xx} 差值越大，二者的绝对值越小。随着传输距离的增加，$\theta(\boldsymbol{\rho}, 0, z)$ 的绝对值逐渐增大，最终趋于一定值；$\theta(\boldsymbol{\rho}, \boldsymbol{\rho}, z)$ 最终趋于初始值。

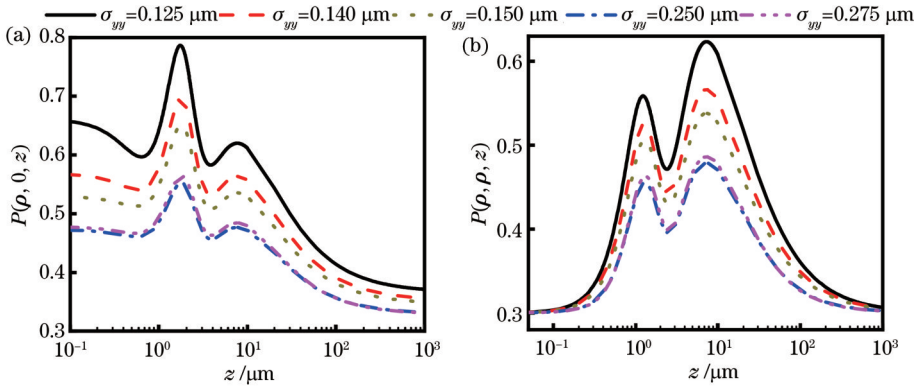

图 7　具有不同空间自相关长度的光束偏振度 P 随 z 的变化。(a)$P(\boldsymbol{\rho}, 0, z)$;(b)$P(\boldsymbol{\rho}, \boldsymbol{\rho}, z)$

Fig. 7　Change of the degree of polarization P with z for beams with different spatial self-correlation lengths. (a) $P(\boldsymbol{\rho}, 0, z)$; (b) $P(\boldsymbol{\rho}, \boldsymbol{\rho}, z)$

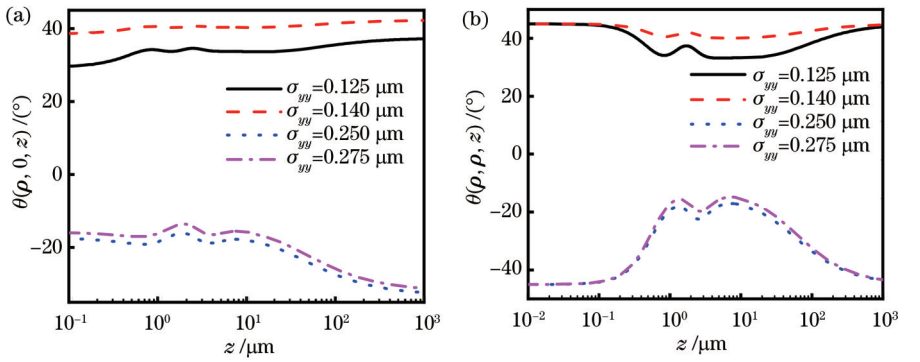

图 8　具有不同空间自相关长度的光束方位角 θ 随 z 的变化。(a)$\theta(\boldsymbol{\rho}, 0, z)$;(b)$\theta(\boldsymbol{\rho}, \boldsymbol{\rho}, z)$

Fig. 8　Change of orientation angle θ with z for beams with different spatial self-correlation lengths. (a) $\theta(\boldsymbol{\rho}, 0, z)$; (b) $\theta(\boldsymbol{\rho}, \boldsymbol{\rho}, z)$

图 9 所示为 $\varepsilon(\boldsymbol{\rho}, 0, z)$ 和 $\varepsilon(\boldsymbol{\rho}, \boldsymbol{\rho}, z)$ 随 z 的变化，计算参数 $\lambda=0.6328$ μm，其他参数同图 1。由图 9 可知，$\varepsilon(\boldsymbol{\rho}, 0, z)$ 的初始值和最终值与 σ_{yy} 的大小有关，$\varepsilon(\boldsymbol{\rho}, \boldsymbol{\rho}, z)$ 最终趋于初始值。由图 9(a)可知：随着传输距离的增加，$\varepsilon(\boldsymbol{\rho}, 0, z)$ 先减小再增大后又稍微减小，最终增加到一大于初始值的定值；在同一传输距离处，$\sigma_{yy}=\sigma_{xx}$ 光束的 $\varepsilon(\boldsymbol{\rho}, 0, z)$ 值最大。由图 9(b)可知，在传输过程中，$\sigma_{yy}=\sigma_{xx}$ 时的 $\varepsilon(\boldsymbol{\rho}, \boldsymbol{\rho}, z)$ 保持一最大的定值，而 $\sigma_{yy}\neq\sigma_{xx}$ 时 $\varepsilon(\boldsymbol{\rho}, \boldsymbol{\rho}, z)$ 具有明显的极大值和极小值。当 $\sigma_{yy}>\sigma_{xx}$ 且大于 0.225 μm 时，σ_{yy} 越大，$\varepsilon(\boldsymbol{\rho}, 0, z)$ 和 $\varepsilon(\boldsymbol{\rho}, \boldsymbol{\rho}, z)$ 的极值越小，且同一传输位置的数值越小。

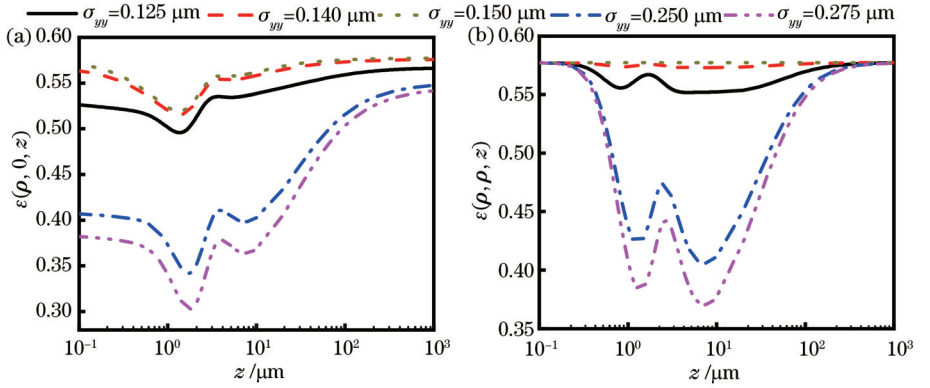

图 9　具有不同空间自相关长度的光束椭圆率 ε 随 z 的变化。(a)$\varepsilon(\boldsymbol{\rho}, 0, z)$;(b)$\varepsilon(\boldsymbol{\rho}, \boldsymbol{\rho}, z)$

Fig. 9　Change of ellipticity ε with z for beams with different spatial self-correlation lengths. (a) $\varepsilon(\boldsymbol{\rho}, 0, z)$; (b) $\varepsilon(\boldsymbol{\rho}, \boldsymbol{\rho}, z)$

4　结　　论

通过推导的部分相干圆刃型位错光束在生物组织传输中的交叉谱密度矩阵元，分析了两类不同场点的光束在人体真皮中的偏振态变化，比较了不同的光束波长、位错数目、空间自相关长度对偏振度、方位角和椭圆率的影响。偏振态的演化趋势是由生物组织湍流引起的，不同参数的光束受湍流的影响不同。结果表

明,光束波长和位错数目不影响偏振态的初始值,而不同空间自相关长度的光束的初始偏振态不同。随着传输距离增加,空间同一点的偏振态经历明显的起伏变化后最终趋于与源处一致,空间不同两点之间的偏振态最终趋于一不同于初始值的定值。比较两种偏振度的变化,无论是初始值还是最终值,不同场点之间的偏振度都大于同一点的偏振度。远红外光在生物组织传输中易发生共振,偏振态在一段传输距离内几乎保持一定值;紫外光被组织强烈吸收,光束偏振态较小;可见光与近红外光的偏振态变化幅度适中,可作为生物医学疾病诊疗的目标光束。位错数目越大,各偏振特征参量极值间距越大。空间自相关长度的相对大小会影响偏振态的大小及变化趋势。在正常生物组织传输中偏振态数值变化的范围,可以作为检测组织是否病变的依据,从而判断组织的病理状态。本文的研究结果将为激光参数的选择提供理论和实验依据,对组织成像技术的发展具有重要意义。

参 考 文 献

[1] Neprokin A, Broadway C, Myllylä T, et al. Photoacoustic imaging in biomedicine and life sciences[J]. Life, 2022, 12(4): 588.

[2] 马志远, 陈康, 张明明, 等. 拉盖尔-高斯幂指数相位涡旋光束传输特性[J]. 光学学报, 2022, 42(5): 0526001.
Ma Z Y, Chen K, Zhang M M, et al. Propagation characteristics of Laguerre-Gaussian power-exponent- phase-vortex beams[J]. Acta Optica Sinica, 2022, 42(5): 0526001.

[3] Shirshin E A, Yakimov B P, Budylin G S, et al. Biomedical photonics for intraoperative diagnostics: review of capabilities and clinical applications[J]. Moscow University Physics Bulletin, 2022, 77(6): 777-800.

[4] 谢家俊, 唐诗瑶, 陈永强, 等. 贝塞尔光束在生物组织中的自重建特性研究[J]. 中国激光, 2022, 49(5): 0507302.
Xie J J, Tang S Y, Chen Y Q, et al. Self-reconstruction characteristics of Bessel beam in biological tissue[J]. Chinese Journal of Lasers, 2022, 49(5): 0507302.

[5] 吕晨阳, 战仁军. 激光辐照下生物组织内光分布理论模型[J]. 激光与光电子学进展, 2021, 58(6): 0600003.
Lü C Y, Zhan R J. Theoretical models of light distribution in biological tissues irradiated by laser[J]. Laser & Optoelectronics Progress, 2021, 58(6): 0600003.

[6] 骆清铭, 龚辉, 刘贤德, 等. 生物组织中激光传输规律的模拟与检验[J]. 光子学报, 1995, 24(2): 125-129.
Luo Q M, Gong H, Liu X D, et al. Simulation and examination of laser propagation in biological tissue[J]. Acta Photonica Sineca, 1995, 24(2): 125-129.

[7] 乔文龙, 周亮, 刘朝晖, 等. 生物组织多光谱偏振特性研究[J]. 光谱学与光谱分析, 2022, 42(4): 1070-1075.
Qiao W L, Zhou L, Liu Z H, et al. Study on multispectral polarization characteristics of biological tissues[J]. Spectroscopy and Spectral Analysis, 2022, 42(4): 1070-1075.

[8] Zhou Y, Cheng K, Sun X, et al. Average intensity and polarization evolution of aberrated partially coherent cosh-Airy beams propagating in ocean turbulence[J]. Journal of Modern Optics, 2022, 69(5): 233-242.

[9] Li Z Y, Luo Y F, Dang A H. Polarization changes of beams travelling through anisotropic turbulence for optics transmission [J]. Proceedings of SPIE, 2018, 10964: 109640O.

[10] Li Y, Gao M. Turbulence-induced changes in the state of polarization of partially polarized, partially coherent pulsed electromagnetic beams propagating through anisotropic turbulence[J]. Optical Engineering, 2019, 58(11): 116107.

[11] 陈康, 厉淑贞, 潘玉琪, 等. 部分相干径向偏振旋转对称幂指数相位涡旋光束紧聚焦特性研究[J]. 光学学报, 2022, 42(22): 2226002.
Chen K, Li S Z, Pan Y Q, et al. Tight focusing properties of partially coherent radially polarized rotationally-symmetric power-exponent-phase vortex beam[J]. Acta Optica Sinica, 2022, 42(22): 2226002.

[12] Soskin M S, Vasnetsov M V. Singular optics[M]//Progress in optics. Amsterdam: Elsevier, 2001: 219-276.

[13] Vasnetsov M V, Gorshkov V N, Marienko I G, et al. Wavefront motion in the vicinity of a phase dislocation: "optical vortex"[J]. Optics and Spectroscopy, 2000, 88(2): 260-265.

[14] Gao P H, Bai L, Li J L. Comparison of propagation properties of circular edge dislocation beams and circular-linear edge dislocation beams[J]. OSA Continuum, 2020, 3(11): 2997-3007.

[15] Liu J Q, Wang J, Yang Z J, et al. Transmission dynamics of circular-linear edge dislocation solitons in nonlocal nonlinear media[J]. Results in Physics, 2022, 42: 105947.

[16] Li J H, Gao P H, Cheng K, et al. Dynamic evolution of circular edge dislocations in free space and atmospheric turbulence[J]. Optics Express, 2017, 25(3): 2895-2908.

[17] Wolf E. Introduction to the theory of coherence and polarization of light[M]. Cambridge: Cambridge University Press, 2007.

[18] 沃尔夫, 蒲继雄. 光的相干与偏振理论导论[M]. 北京: 北京大学出版社, 2014.
Wolf E, Pu J X. Introduction to the theory of coherence and polarization of light[M]. Beijing: Peking University Press, 2014.

[19] 段美玲, 杜娇, 赵志国, 等. 部分相干圆刃型位错光束在生物组织中的动态演化[J]. 光子学报, 2021, 50(9): 0929001.
Duan M L, Du J, Zhao Z G, et al. Dynamic evolution of the patically coherent circular edge dislocation beams propagating in biological tissues[J]. Acta Photonica Sinica, 2021, 50(9): 0929001.

[20] Ishimaru A. Phase fluctuations in a turbulent medium[J]. Applied Optics, 1977, 16(12): 3190-3192.

[21] Andrews L C, Phillips R L. Laser Beam Propagation through Random Media[M]. Bellingham: SPIE Press, 2005.

[22] Zauderer E. Complex argument Hermite-Gaussian and Laguerre-Gaussian beams[J]. Journal of the Optical Society of America A, 1986, 3(4): 465-469.

[23] Schmitt J M, Kumar G. Turbulent nature of refractive-index variations in biological tissue[J]. Optics Letters, 1996, 21(16): 1310-1312.

[24] Wang S C H, Ouyang C F, Plonus M A. Optical beam propagation for a partially coherent source in the turbulent atmosphere[J]. Journal of the Optical Society of America, 1979, 69(9): 1297-1304.

[25] Gradshteyn I S, Ryzhik I M. Table of integrals, series and products[M]. New York: Academic Press, 2014.

[26] Ji X L, Chen X W. Changes in the polarization, the coherence and the spectrum of partially coherent electromagnetic Hermite-Gaussian beams in turbulence[J]. Optics & Laser Technology, 2009, 41(2): 165-171.

[27] Korotkova O, Salem M, Dogariu A, et al. Changes in the polarization ellipse of random electromagnetic beams propagating through the turbulent atmosphere[J]. Waves in Random and Complex Media, 2005, 15(3): 353-364.

[28] 赵柯莹, 李晋红, 赖云忠. 随机电磁光束在大气湍流中偏振态的变化[J]. 光电子·激光, 2015, 26(4): 812-818.
Zhao K Y, Li J H, Lai Y Z. Changes of the polarization states of random electromagnetic beams in atmospheric turbulence[J]. Journal of Optoelectronics·Laser, 2015, 26(4): 812-818.

[29] Westphal V, Hell S W. Nanoscale resolution in the focal plane of an optical microscope[J]. Physical Review Letters, 2005, 94(14): 143903.

Polarization Properties of Partially Coherent Circular Edge Dislocation Beams in Biological Tissue

He Gaimei, Duan Meiling*, Yin Ziang, Shan Jing, Feng Jiaojiao

School of Semiconductor and Physics, North University of China, Taiyuan 030051, *Shanxi, China*

Abstract

Objective Due to the rapid development of laser optics, the application of optical methods in photoacoustics, photoacoustic imaging, biomedicine photonics, and other fields has received widespread attention presently. As is known, it is significant to study the propagation behaviors of lasers in biological tissue to understand the interaction mechanism between the laser and biological tissue. Up to now, a large number of researchers have studied the polarization behavior of laser beams propagating through different media, such as ocean turbulence, atmospheric turbulence, and free space. In addition, the circular edge dislocation beam belongs to a typical singular beam with a circular notch in the transverse plane along the transmission direction, which undergoes a π mutation in the phase across the notch (dislocation line), and the basic research about the polarization state of circular edge dislocation beams in biological tissue transmission has not been reported yet. In order to promote the application of singularity optics in biomedical disease diagnosis and treatment and the development of tissue imaging technology, the basic research on the polarization behavior of circular edge dislocation beams in biological tissue transmission has been studied in this work, and the effects of different beam parameters (wavelength, number of dislocations, and spatial self-correlation length) on the changes in polarization state for different field points have been analyzed and compared in detail. We hope that the obtained results in this work will provide theoretical and experimental guidance for the selection of laser parameters in different applications and enhance the development of tissue imaging technology.

Methods By introducing the Schell term, the cross spectral density matrix of partially coherent circular edge dislocation beams is obtained by the field distribution of the circular edge dislocation beams at the source. Based on the generalized Huygens-Fresnel principle, the analytical expression of the cross spectral density matrix element of partially coherent circular edge dislocation beams propagating biological tissue is derived with the help of the properties of the Hermite function and the complex integration. By means of the unified theory of coherence and polarization, the change in the degree of polarization, orientation angle, and ellipticity of partially coherent circular edge dislocation beams in biological tissue transmission can be investigated by numerical simulation, respectively. Meanwhile, the effects of different beam parameters (beam wavelength, number of dislocations, and spatial self-correlation length) can be analyzed during the transmission process.

Results and Discussions Numerical calculations show that the magnitude of wavelength and dislocations number of partially coherent circular edge dislocation beams do not affect the initial value of the beam polarization state (Figs. 1-6), while the initial polarization state of beams with different spatial self-correlation length is different (Figs. 7-9). With the increment of propagation distance, the value of the polarization state of the same field point will eventually tend to be consistent with the initial one after experiencing obvious fluctuations, and those between two different field points will eventually move to a fixed one that is different from the initial value (Figs. 1-9), respectively, which may due to the impact of biological tissue turbulence on polarization behaviors. By comparing the changes in polarization between two situations, both the initial and final values show that the difference between two different field points is greater than that of the same field point (Figs. 1, 4, and 7). Far infrared light is prone to resonance in biological tissue transmission, and the polarization state remains almost constant over a certain transmission distance. Ultraviolet light is strongly absorbed by the tissue, and the polarization state of the beam is relatively small. The polarization changes of visible light and near-infrared light are moderate and can be used as probe beams for biomedical disease diagnosis and treatment (Figs. 1-3). A larger dislocation number indicates a greater distance between the extreme values of each polarization characteristic parameter (Figs. 4-6). The relative size of spatial self-correlation length will play a big role in the size and change trend of the polarization state (Figs. 7-9). It can be seen that beams with different beam parameters will have different turbulence resistance abilities, and different beams should be applied in different fields.

Conclusions In the present study, based on the generalized Huygens-Fresnel principle and the unified theory of coherence and polarization, the influence of different beam parameters on the change in polarization state between two kinds of field points is numerically simulated. The obtained results indicate that compared with far-infrared and ultraviolet

light, both visible light and near-infrared light are more suitable as probe beams for biomedical disease diagnosis and treatment. Affected by the turbulence of biological tissue, the polarization state of the beam undergoes evident fluctuations. The beams with different beam parameters have different turbulence resistance abilities, so beams with different parameters will be selected for different applications. The research results obtained in this work will provide a theoretical and experimental guide for the selection of laser parameters and are of great significance for the development of tissue imaging technology.

Key words bi-optics; circular edge dislocation beam; degree of polarization; orientation angle; ellipticity; biological tissue